sup. Fig. 1

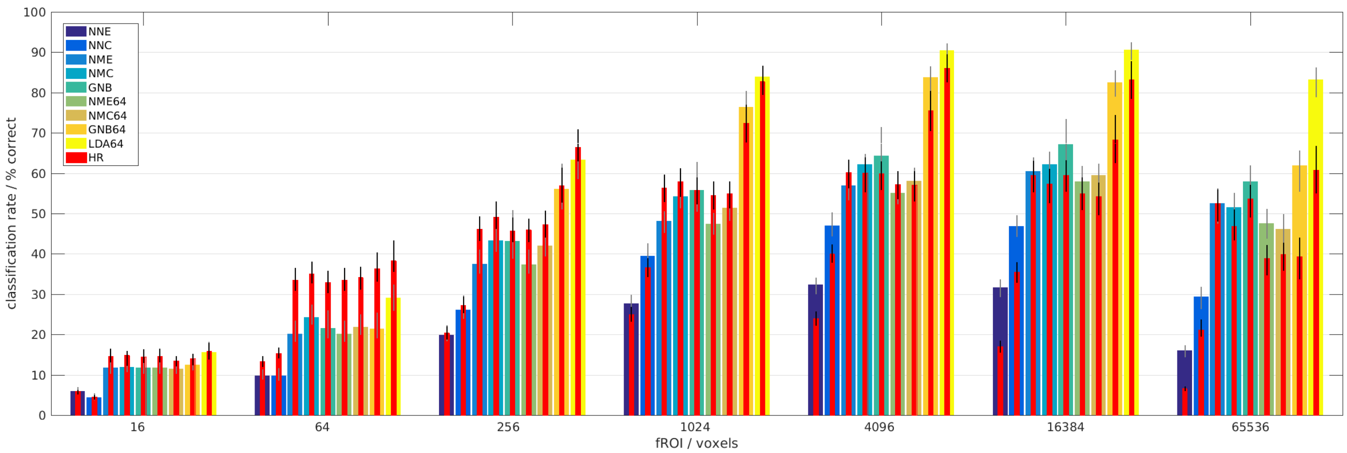

Figure 1 Classifier comparison

In analogy to Figure 3: The classification accuracy (y-axis) for 6 different classifiers (colors, see Table 1) had a similar dependence on fROI size (x-axis) and fMRI resolution (LR/HR = wide/narrow bars), despite obvious differences in overall sensitivity. (Errorbars = 100x bootstrap.)

NNE	nearest-neighbour (NN) by Euclidean distance
NNC	NN by correlation distance
NME	nearest-mean (NM) by Euclidean distance
NMC	NM by correlation distance
GNB	Gaussian Naïve Bayes (NM by normalized Euclidean distance)
GNB64	Gaussian Naïve Bayes using 64 principal components (PCs)
LDA64	Linear Discriminant Analysis (NM by Mahalanobis distance) using 64 PCs

sup. Fig. 2

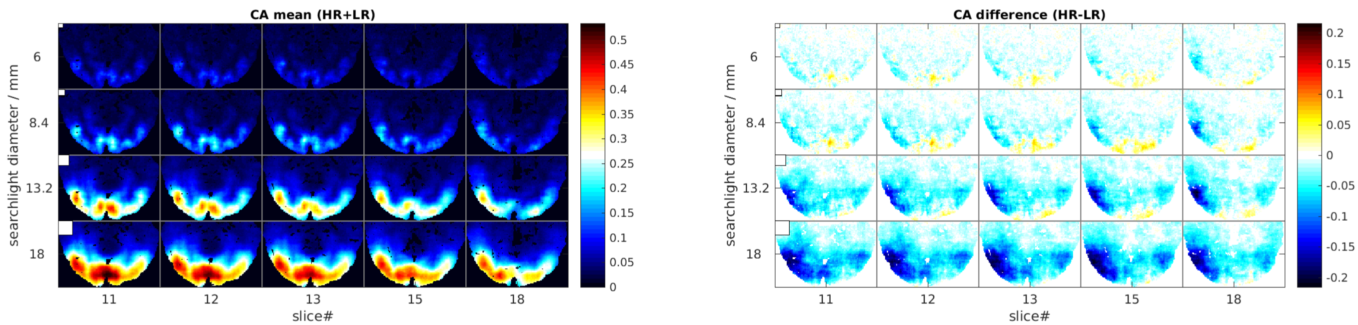

Figure 2 Searchlight CA as a function of SL volume

Mean (HR+LR) (left panel) and difference (HR-LR) (right panel) in Searchlight CA (NMC classifier) for SL volumes of (6-18mm)^3 (rows). Five slices (columns) in one representative subject showing higher CA at high resolution mostly in early visual areas only.

sup. Fig. 3

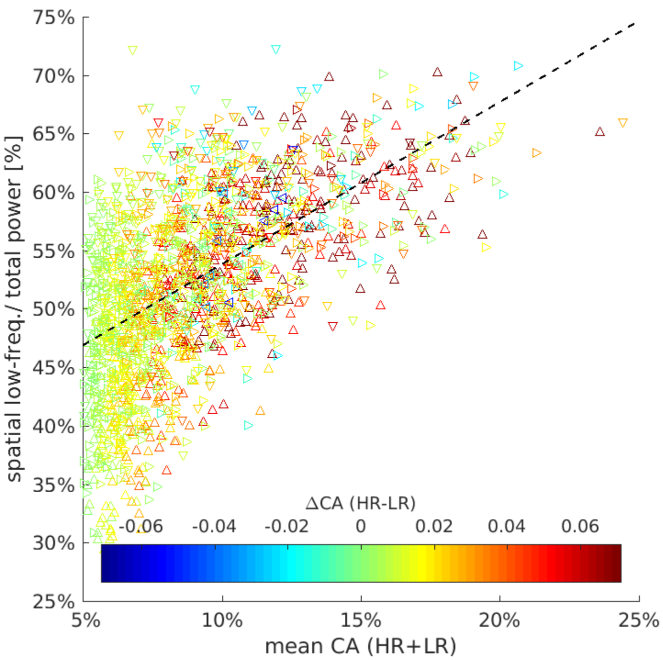

Figure 3 High searchlight CA correlated with a locally smooth BOLD signal.

Each marker represents one SL volume in one of four subjects: There is a significant correlation between the mean CA (HR+LR) (x-axis) and the proportion (%) of power in the lower half of the spatial spectrum of HR data (y-axis). Marker colors represent the local difference in CA (HR-LR). SL volumes with CA < 5% for either HR or LR data were excluded.

Fig. 4

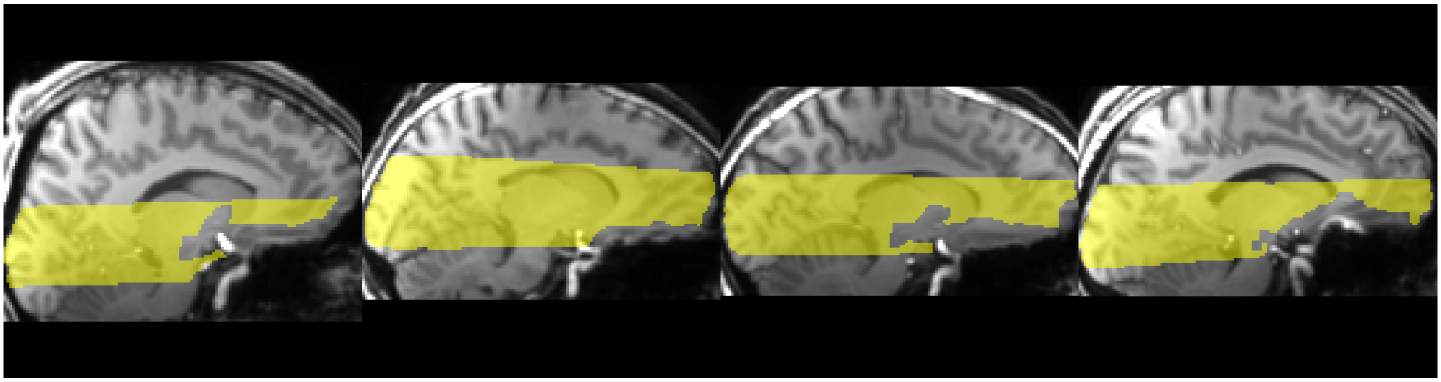

subject 1	subject 2	subject 3	subject 4
LR: 71699 vox.	78473 vox.	90705 vox.	65191 vox.
HR: 53675 vox.	47050 vox.	45872 vox.	30904 vox.

Figure 4 fMRI FOV over a T1-weighted anatomy of each subject

The yellow masks delineate the axial section covered consistently by all fMRI experiments in each subject. Frontal regions suffering from susceptibility artifacts were excluded from the classification analysis. Maximal fROI = total number of voxels (in posterior half) significantly modulated by the movie stimulus (ANOVA p(F)<1% uncorrected) in LR and HR data.

sup. Fig. 5

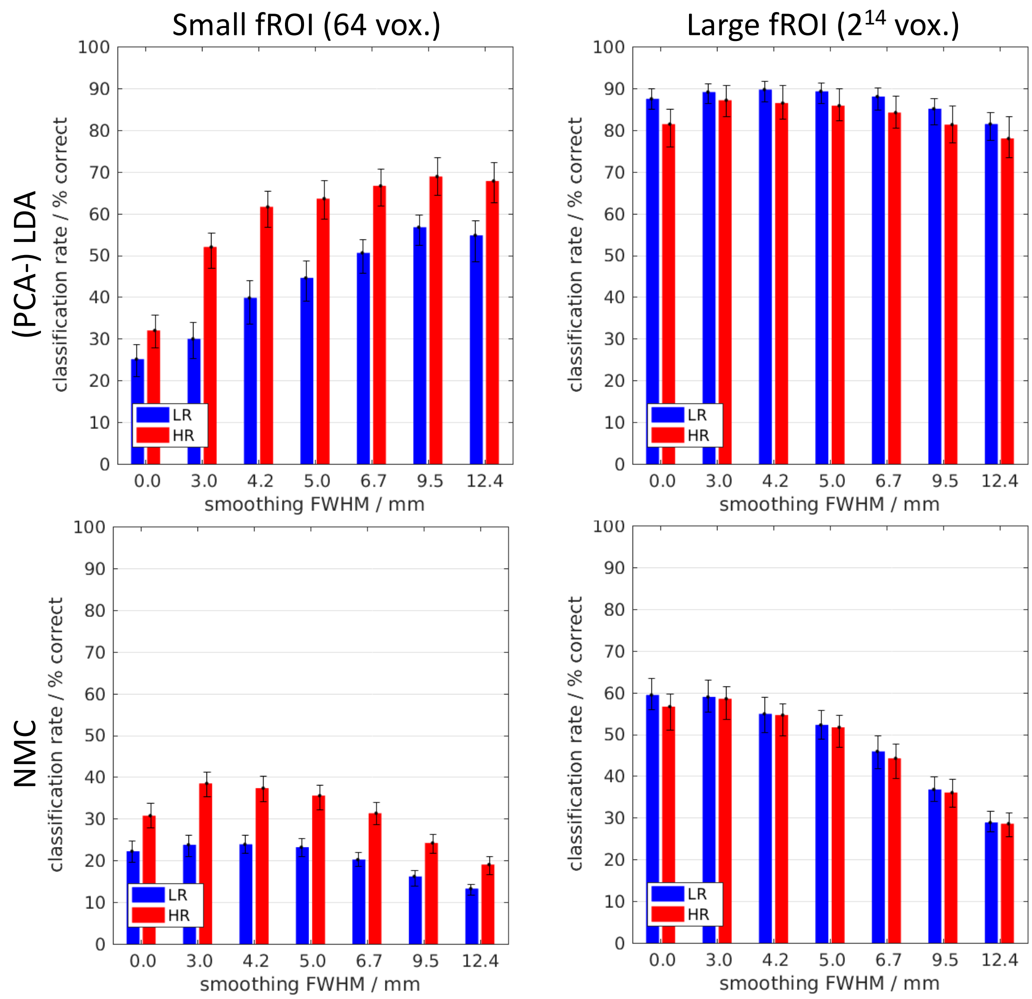

Figure 5 Effects of resolution and smoothing depended on fROI size

For small fROIs (left panels) high-resolution fMRI data (red) yielded higher classification accuracy (y-axes) than low-resolution data (blue), especially after smoothing (x-axes), nota bene. The PCA-regularized LDA classifier (top panels) profited from Gaussian smoothing (x-axes) much more than the correlation-distance (nearest-mean) classifier (NMC, bottom panels).

sup. Fig. 6

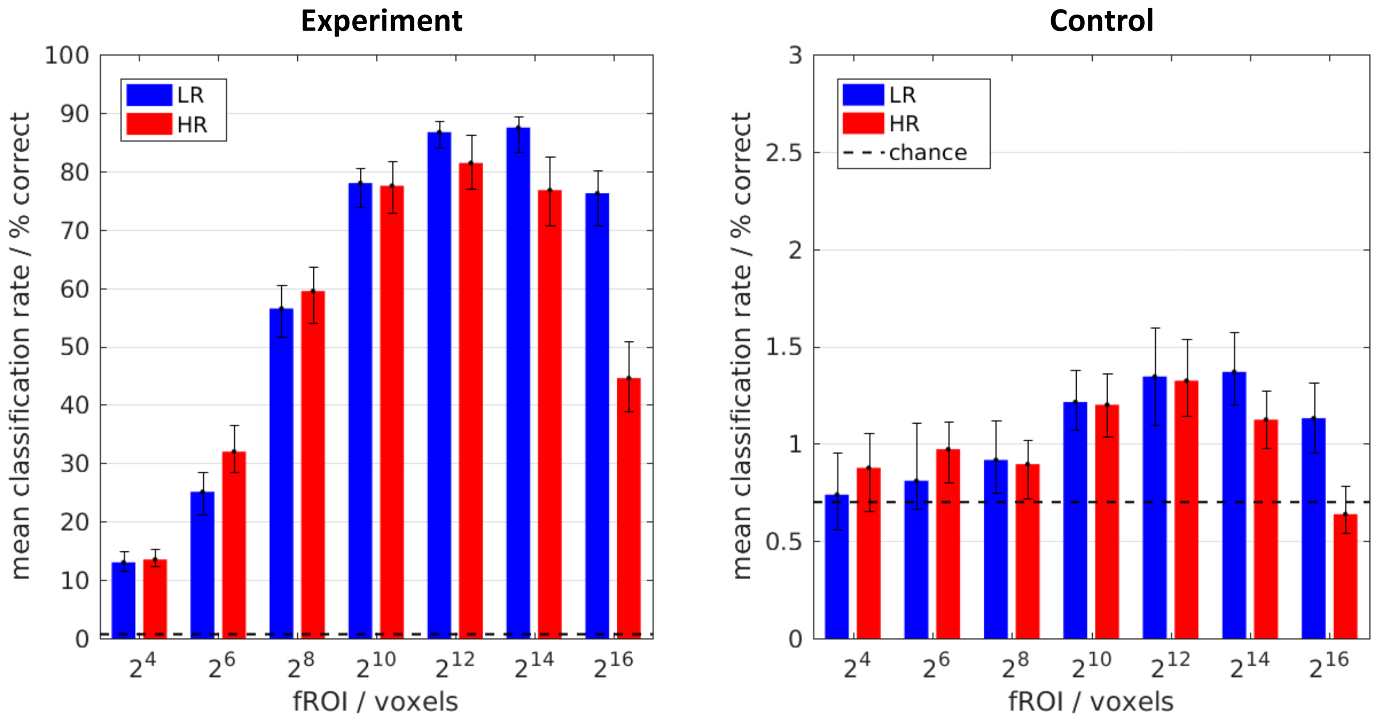

Figure 6 The theoretical chance level of 1/150 was confirmed by a control analysis (right)

Left: The classification accuracy (y-axis) achieved by an LDA classifier reached a maximum for a large, global input fROI comprising 2^14 voxels (x-axis) and the lower fMRI resolution of 2mm (blue bars). The high-resolution fMRI data (1.2mm, red bars) supported equal or better discriminability only for smaller (sub-optimal) input ROIs (<1000 voxels). Error bars span a 95% confidence interval around the mean computed by 100-fold bootstrap. Right: As a control, cross-classification between different movie stimuli yielded classification accuracies within 1% of the theoretical chance level (1/150). (Note the different y-scales!)

sup. Fig. 7

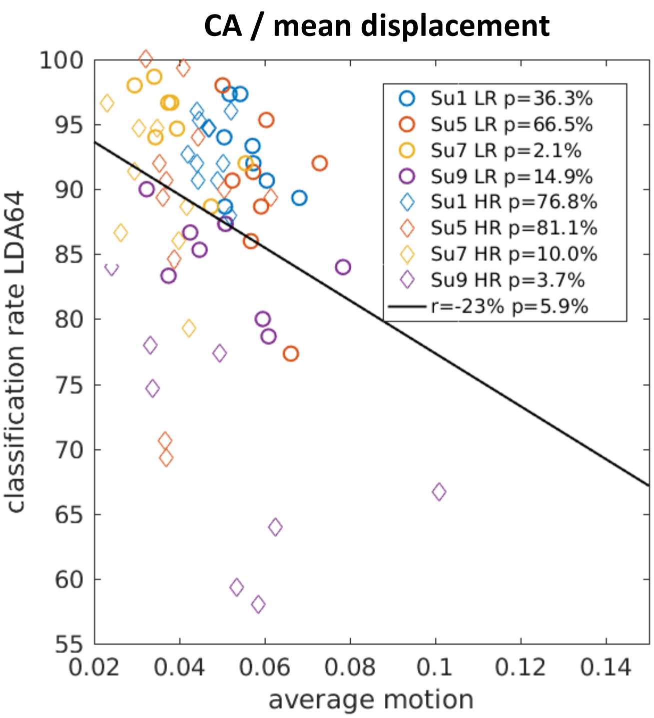

Figure 7 Non-significant correlation between classification accuracy and subject motion

The average (RMS) voxel displacement values calculated as part of the motion correction algorithm (mcflirt, FSL) did show some variation across subjects and experiments, but not enough to systematically explain a significant amount of variance in classification accuracy: The Spearman rank correlation coefficients (r) were not significant (p>5%) for (almost) all subjects (Su1-4) and resolutions (LR/HR = **O**/◆).